Supplementary Figure 1: AAV capsid library outcome post round-2 *in vivo* selection

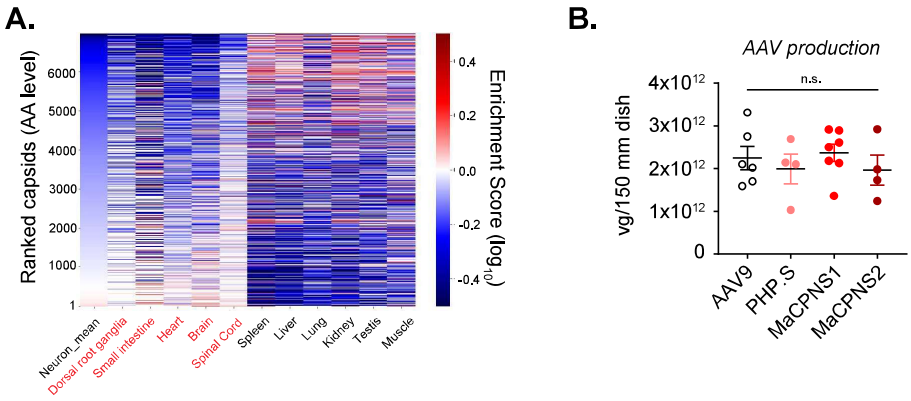

Supplementary Figure 1: AAV capsid library outcome post round-2 *in vivo* selection. Related to Figure 1.

A. Heatmap of 6300 capsid variants which showed a bias towards one or more of the neuronal tissues. Heatmap shows mean enrichment by Cre-dependent recovery across tissues of interest (red text) and Cre-independent recovery across off-targets (black text) after two rounds of selection. Cre lines are grouped by organs. The y-axis represents capsids unique at the amino acid (AA) level, ranked by 'neuron mean', which is the mean of the enrichment of all targets of interest. **B.** AAV vector yields from an established laboratory protocol (see Methods). One-way analysis of variance (ANOVA) non-parametric Kruskal-Wallis test (approximate P=0.6407, n.s.), and follow-up multiple comparisons with uncorrected Dunn's test are reported (individual P > 0.05, n.s.; n≥4 per group, each data point is the mean of 3 technical replicates, mean ± s.e.m is plotted).

Supplementary Figure 2: Characterization of AAV variants across different organs in mice following systemic delivery.

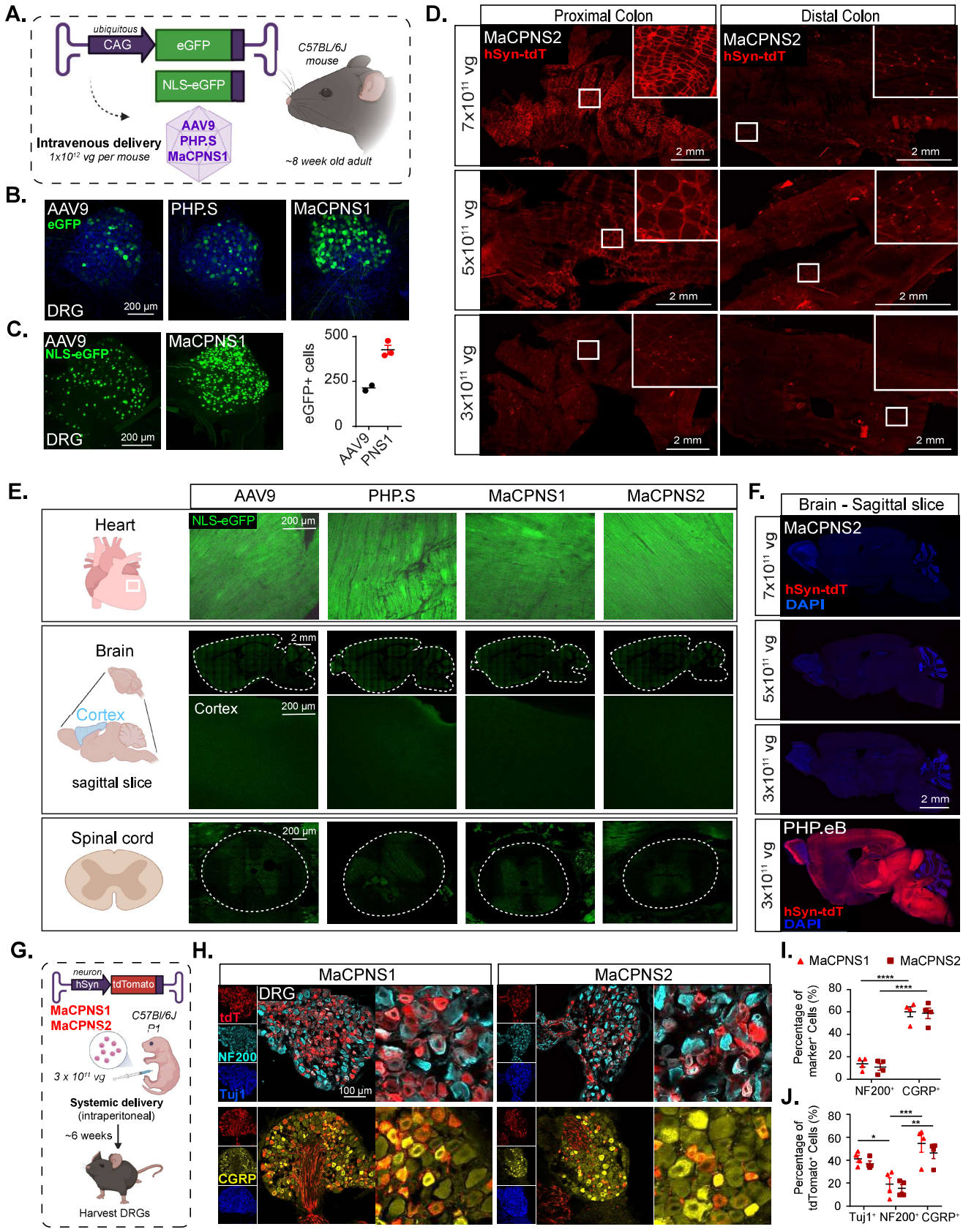

Supplementary Figure 2: Characterization of AAV variants across different organs in mice following systemic delivery. Related to Figure 2.

A. Illustration of IV administration of AAV9/PHP.S/MaCPNS1 capsid packaged with either ssAAV:CAG-eGFP or ssAAV:CAG-NLS-eGFP genome in mice (~8 weeks old, C57BL/6J males) at $1x10^{12}$ vg dose/mouse. **B**. Vector (AAV9/PHP.S/MaCPNS1)-mediated expression of eGFP (green) in DRG after 3 weeks of expression *in vivo* (n=3 per group). **C.** Vector-mediated expression of NLS-eGFP (green) in DRG after 3 weeks of expression, with imaging parameters matched across samples. Quantification of eGFP+ cells in DRG is shown at right (n=2-3 per group, mean ± s.e.m is plotted for n>2, mean is plotted for n=2). **D.** MaCPNS2 vector-mediated expression of tdTomato (red) from ssAAV:hSyn-tdTomato in the proximal and distal segments of the colon at three different IV doses per mouse: $7x10^{11}$ vg, $5x10^{11}$ vg, $3x10^{11}$ vg (3 weeks of expression, n=3 per group, white boxes show zoomed-in views of selected areas). **E.** Vector (AAV9, PHP.S, MaCPNS1 and MaCPNS2)-mediated expression of NLS-eGFP (green) in organs after 3 weeks of expression. Top panels show expression in heart. Middle panels show expression in the brain with zoomed-in views of the cortex. Bottom panels show expression in the spinal cord. **F.** MaCPNS2 vector-mediated expression of tdTomato (red) from ssAAV:hSyn-tdTomato in the brain at three different IV doses per mouse: $7x10^{11}$ vg, $5x10^{11}$ vg, $3x10^{11}$ vg (3 weeks of expression, n=3 per group). Bottom panel shows PHP.eB vector-mediated expression of tdTomato (red) using ssAAV:hSyn-tdTomato in the brain at an IV dose per mouse of $3x10^{11}$ vg (3 weeks of expression, n=3 per group). The tissues were co-stained with the nuclear stain DAPI (blue). Imaging parameters in **B-F** were matched across samples to the respective control in the experiment or the area. **G.** Illustration of intraperitoneal administration of MaCPNS1 vector packaged with ssAAV:hSyn-tdTomato in a C57BL/6J mouse model (postnatal stage 1 (P1), males, $3x10^{11}$ vg IV dose/mouse). After six weeks of expression, the DRG were harvested. **H.** Representative images of DRG sections showing MaCPNS1 vector-mediated tdTomato (red) expression. The tissues were co-stained with αNF200 (cyan), αTuj1 (blue) and αCGRP (yellow) markers. **I.** Quantification of the proportion of αNF200 and αCGRP marker+ cells that overlap with the AAV-mediated tdTomato-expressing cells in DRG, and **J.** proportion of AAV-mediated tdTomato-expressing cells that overlap with αTuj1, αNF200 and αCGRP markers in DRG (n=4 per group, unpaired t-test. Mean+/- sem are shown.)

Supplementary Figure 3: Novel variants transduce peripheral ganglia and CNS in rats.

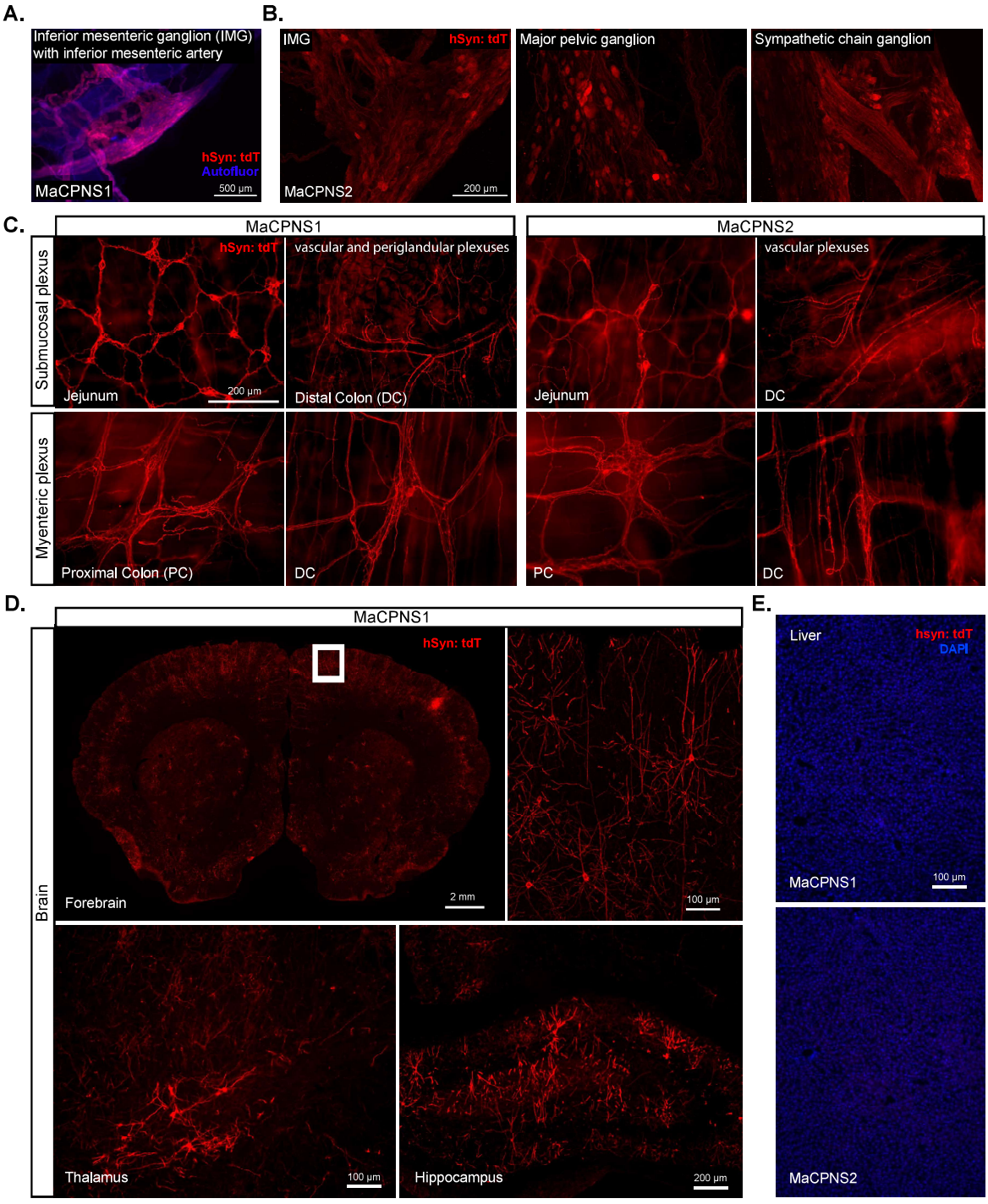

Supplementary Figure 3. Novel variants transduce peripheral ganglia and CNS in rats. Related to Figure 3.

AAV capsids (MaCPNS1 and MaCPNS2 packaged with ssAAV:hSyn-tdTomato genome) were intravenously administered in a rat model (young adults, Sprague Dawley, male, $2x10^{13}$ vg/kg per rat). The tissues were stained with αDsRed (red) antibody against tdTomato. **A.** Representative image of MaCPNS1 vector-mediated tdTomato (red) expression in inferior mesenteric ganglion with inferior mesenteric artery (scale bar: 500 μm). **B**. Representative images of MaCPNS2 vector-mediated tdTomato (red) expression in major pelvic ganglia (left), sympathetic chain ganglia (middle) and inferior mesenteric ganglia (right) in adult rats after 3 weeks of expression (n≥2 per group, scale bar: 200 μm). **C.** Representative images of MaCPNS1 (left) and MaCPNS2 (right) vector-mediated tdTomato expression in the jejunum and distal colon at the submucosal plexus layer (top) and proximal colon and distal colon at the myenteric plexus layer (bottom). (scale bar: 200 μm). **D.** Representative images of MaCPNS1 vector-mediated tdTomato expression in the brain including forebrain (top left, scale bar: 2mm) with zoomed-in view of the cortex (white box, scale bar: 100 μm), thalamus (bottom left, scale bar: 100 μm) and hippocampus (bottom right, scale bar: 200 μm). **E.** Representative images of MaCPNS1 and MaCPNS2 vector-mediated tdTomato expression in the liver. The tissues were co-stained with DAPI (blue) (scale bar: 100 μm).

Supplementary Figure 4: Cell-type profiles of engineered AAVs in marmoset brain

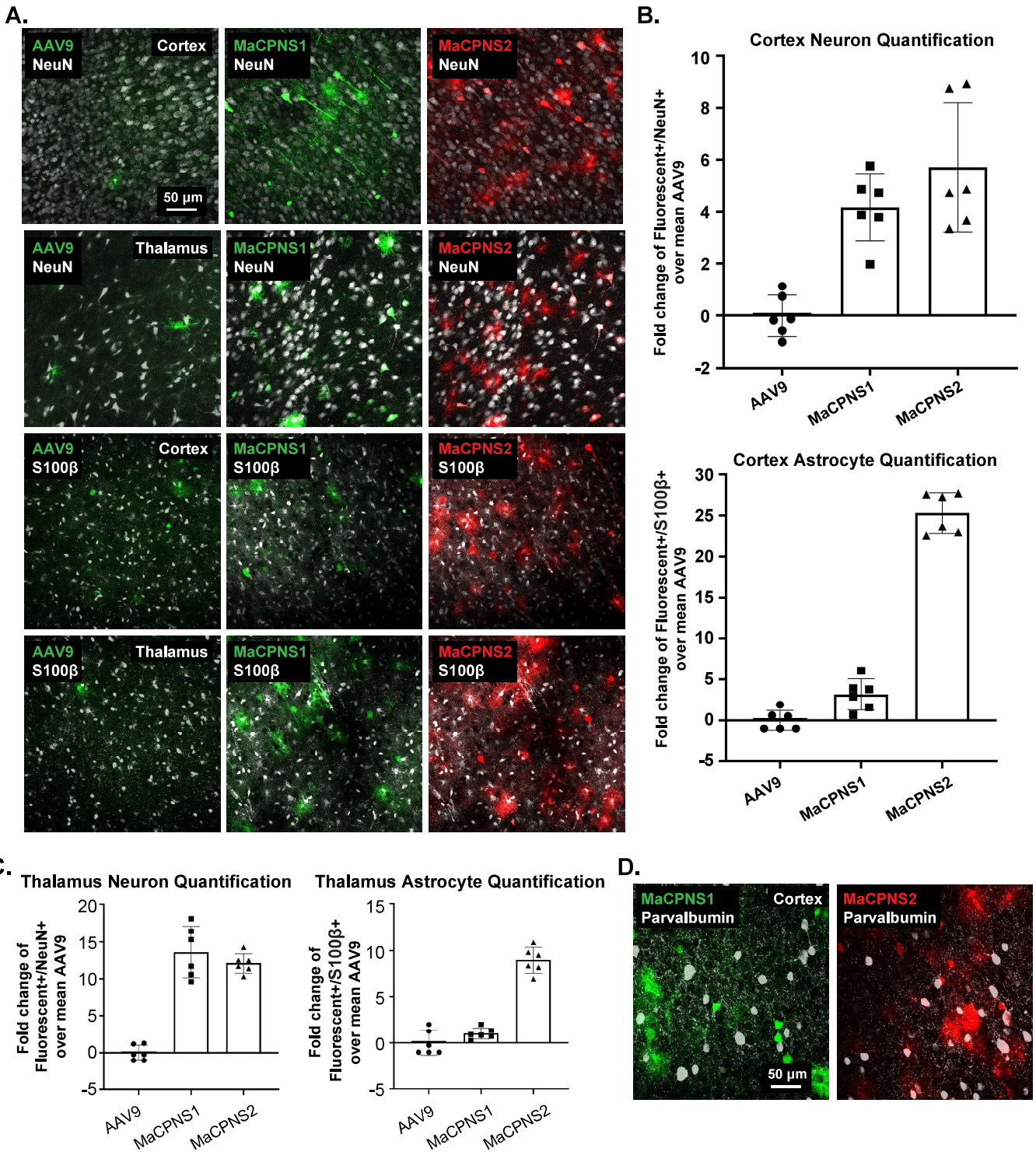

Supplementary Figure 4. Cell-type profiles of engineered AAVs in marmoset brain. Related to Figure 5.

A. Representative images of AAV9, MaCPNS1 and MaCPNS2 vector-mediated fluorescent protein expression in the marmoset cortex and thalamus (scale bar: 50 μm). Slices were co-stained with NeuN (top 2 rows, white) or S100β (bottom 2 rows, white). **B, C.** Quantification of the fold change of Fluorescent+/marker over mean AAV9 in cortex and thalamus. Each data point is a slice. **D.** Representative images of MaCPNS1 and MaCPNS2 vector-mediated fluorescent protein expression in the marmoset cortex (scale bar: 50 μm). Slices were co-stained with Parvalbumin (white).

Supplementary Figure 5 : Engineered vectors transduce spinal cord and DRG in macaque efficiently

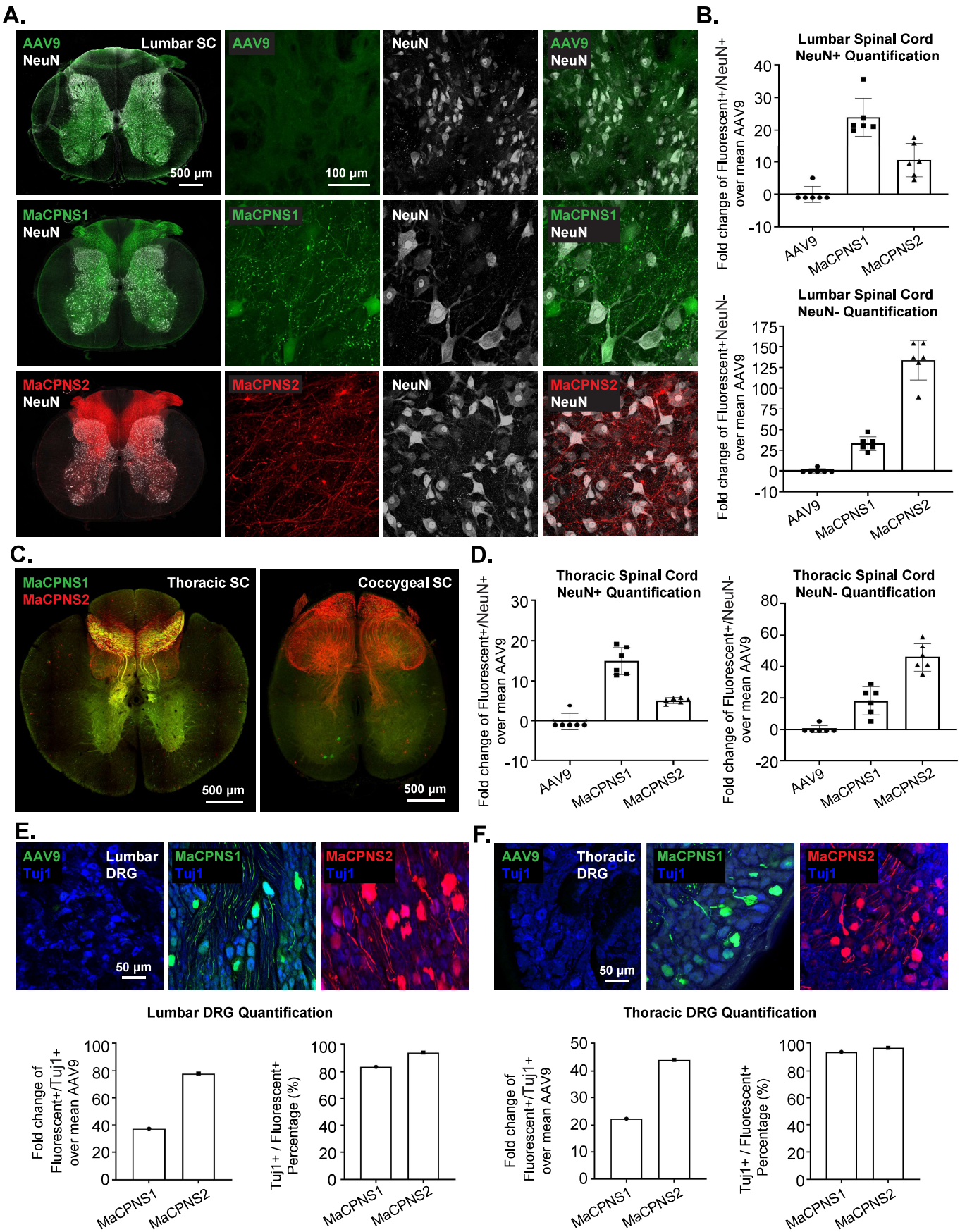

Supplementary Figure 5. Engineered vectors transduce spinal cord and DRG in macaque efficiently. Related to Figure 6.

A. Representative images of AAV9, MaCPNS1 and MaCPNS2 vector-mediated fluorescent protein expression in the macaque lumbar spinal cord (scale bar: 500 μm) with zoomed-in views of each channel (scale bar: 100 μm). Slices were co-stained with NeuN (white). **B.** Quantification of the fold change of Fluorescent+/marker over mean AAV9 in lumbar spinal cord. Each data point is a slice. **C.** Representative images of MaCPNS1 and MaCPNS2 vector-mediated fluorescent protein expression in the macaque thoracic spinal cord and coccygeal spinal cord (scale bar: 500 μm). **D.** Quantification of the fold change of Fluorescent+/marker over mean AAV9 in thoracic spinal cord. Each data point is a slice. **E, F.** (Top Panel) Representative images of AAV9, MaCPNS1 and MaCPNS2 vector-mediated fluorescent protein expression in the macaque lumbar DRG and thoracic DRG (scale bars: 50 μm). Slices were co-stained with Tuj1 (blue). (Bottom Panel) Quantification of the fold change of Fluorescent+/marker over mean AAV9 in DRGs and percentage of Tuj1+ within the fluorescent+ population. Each data point is a slice.

Supplementary Figure 6: Novel variants efficiently transduce macaque CNS while maintaining similar transduction in liver comparing to AAV9

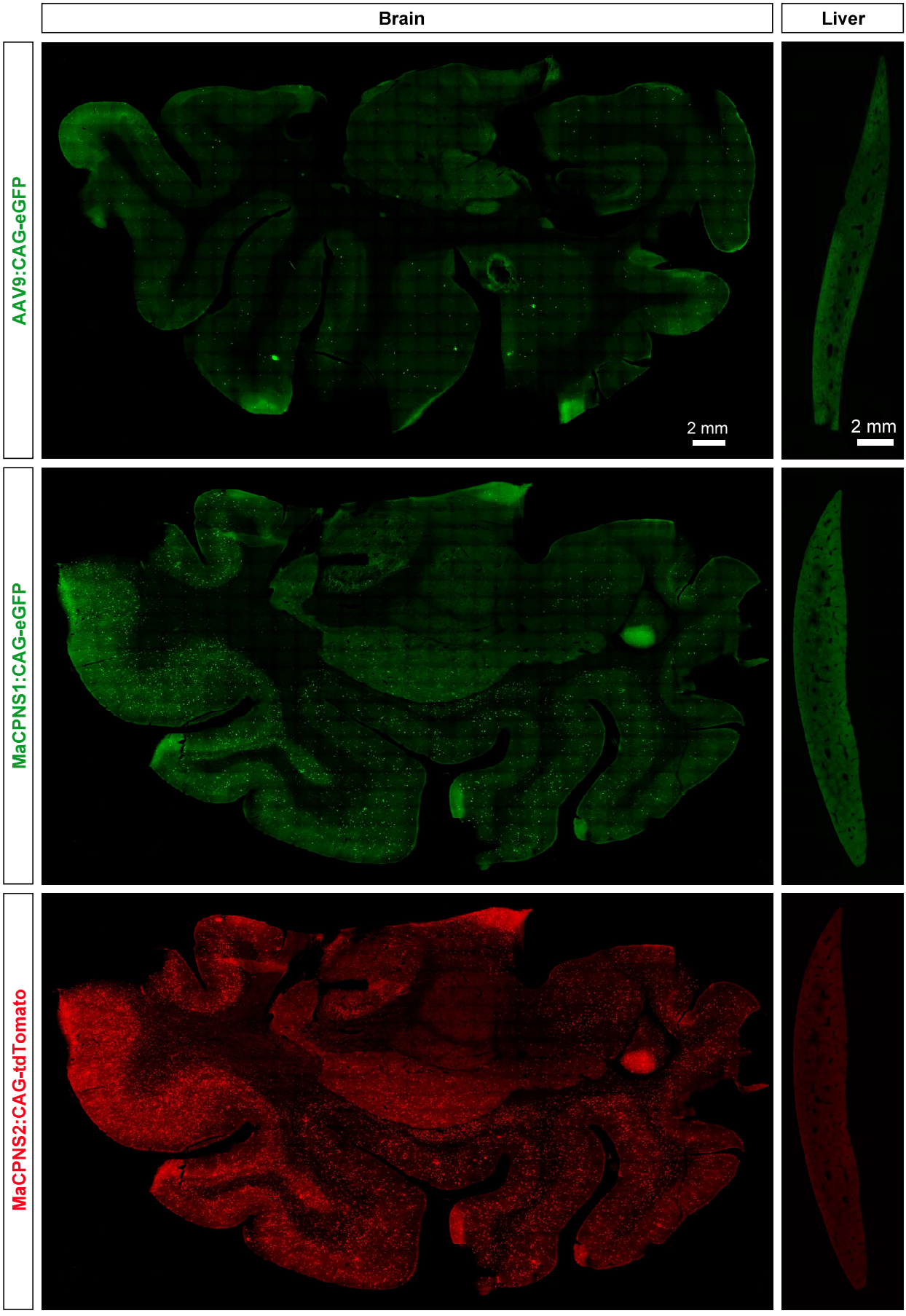

Supplementary Figure 6. Novel variants efficiently transduce macaque CNS while maintaining similar transduction in liver compared to AAV9. Related to Figure 6.

AAV capsids (AAV9/MaCPNS1/MaCPNS2) and their corresponding genomes (ssAAV:CAG-eGFP/tdTomato) were delivered to macaque to study transduction across the CNS and PNS after 3 weeks of expression. Two AAVs packaged with different fluorescent proteins were mixed and intravenously injected at a dose of $5x10^{13}$ vg/kg per macaque (*Macaca mulatta*, female, injected within 10 days of birth, $2.5x10^{13}$ vg/kg per AAV). Representative images of the brain (left) and liver (right) are shown (scale bars: 2 mm).

Supplementary Figure 7 : Cell-type profiles of engineered AAVs in macaque brain

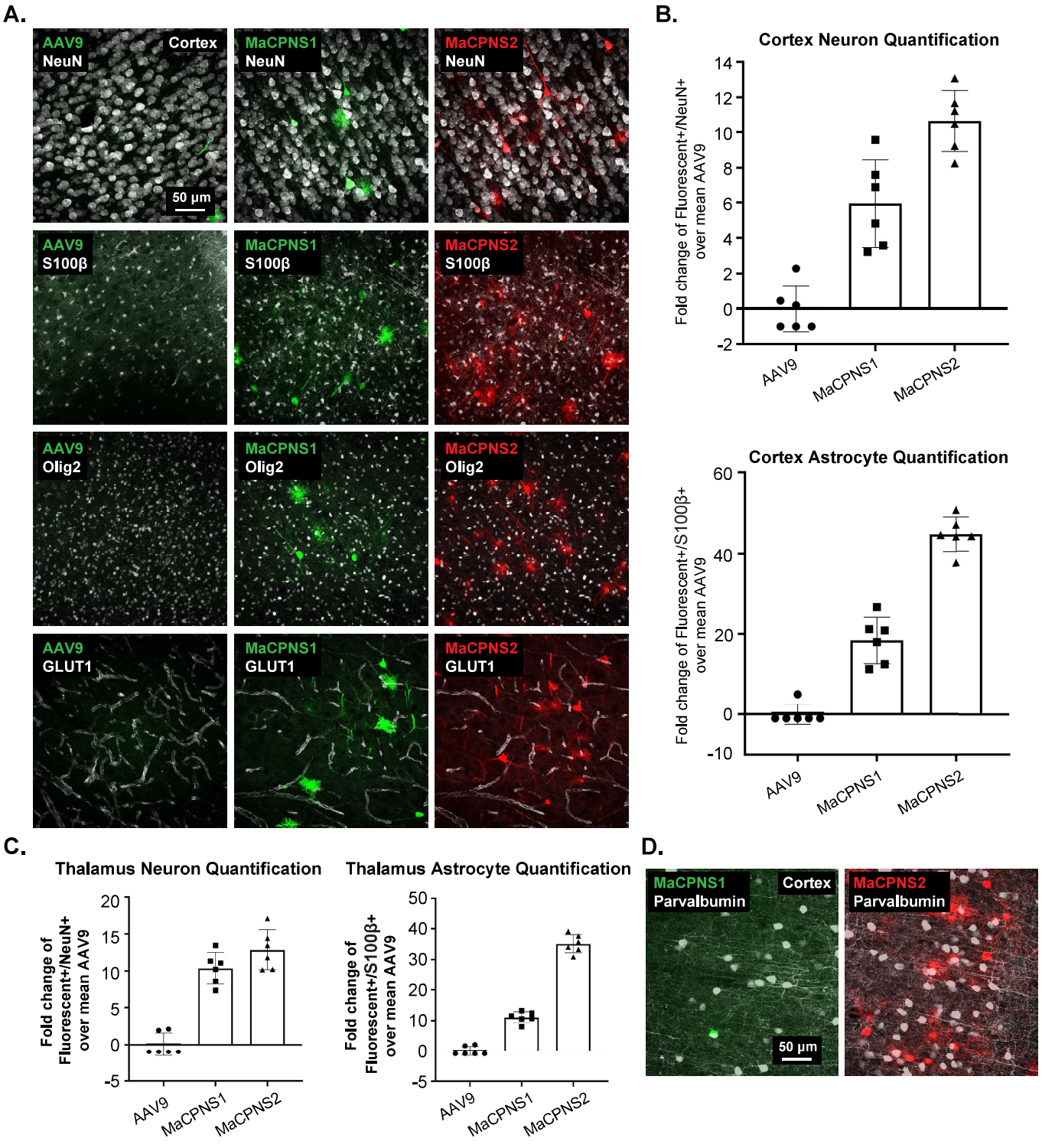

Supplementary Figure 7. Cell-type profiles of engineered AAVs in macaque brain. Related to Figure 6.

A. Representative images of AAV9, MaCPNS1 and MaCPNS2 vector-mediated fluorescent protein expression in the macaque cortex and thalamus (scale bar: 50 μm). Slices were co-stained with NeuN (first row, white), S100β (second row), Olig2 (third row) or GLUT1 (fourth row). **B, C.** Quantification of the fold change of Fluorescent+/marker over mean AAV9 in cortex and thalamus. Each data point is a slice. **D.** Representative images of MaCPNS1 and MaCPNS2 vector-mediated fluorescent protein expression in the macaque cortex (scale bar: 50 μm). Slices were co-stained with Parvalbumin (white).

Table S1. Main features of novel AAVs across species following systemic delivery.

	Mouse	Rat	Marmoset	Macaque
MaCPNS1	• efficient transduction of sensory ganglia (NG/DRG) • demonstrated functional readout and modulation of sensory ganglia	• transduction of sensory ganglia (DRG/TG), sympathetic chain ganglia, mixed sympathetic-parasympathetic ganglia and enteric ganglia across SI and LI • transduction of sensory nerve fibers entering SC and ascending afferent tracts in dorsal column • observed labeling of neurons across brain	• enhanced transduction of DRG, SI and ascending fiber tracts in dorsal column of the SC • robust transduction of neurons and astrocytes • more biased to neurons in the brain	• enhanced transduction of DRG • transduction of sensory nerve fibers entering SC and ascending afferent tracts in dorsal column • robust transduction of neurons and non-neuronal cells in brain and SC • more biased to neurons
MaCPNS2	• efficient transduction of sensory ganglia (NG/DRG) • efficient transduction of ENS, especially SI	• transduction of sensory ganglia (DRG/TG), sympathetic chain ganglia, mixed sympathetic-parasympathetic ganglia and enteric ganglia across SI and LI • transduction of sensory nerve fibers entering SC and ascending afferent tracts in dorsal column • observed labeling of neurons across brain	• enhanced transduction of DRG, SI and ascending fiber tracts in dorsal column of the SC • robust transduction of neurons and astrocytes in the brain	• enhanced transduction of DRG and GI tract, including esophagus, colon and SI • transduction of sensory nerve fibers entering SC and ascending afferent tracts in dorsal column • robust transduction of neurons and non-neuronal cells in brain and SC

NG: nodose ganglia; DRG: dorsal root ganglia; SI: small intestine; LI: large intestine; SC: spinal cord.

Table S1. Main features of novel AAVs across species following systemic delivery, related to Figure 6.